and $\delta(^1H)$, the correlation coefficient being for the van der Waals radii $r_{^{13}C} = 0.995$ and $r_{^1H} = 0.988$, while for electronegativities $r_{^{13}C} = 0.990$ and $r_{^1H} = 0.980$. The van der Waals radius correlation may suggest a very subtle steric effect, but the B–N bond is the strongest in the case of $Me_3N{\cdot}BI_3$, the sterically most crowded structure.

The extent of the NMR and other interrelations suggests that the $Me_3N{\cdot}BXYZ$ (X, Y, and Z are halogens) system would be appropriate for theoretical study in order to account for these phenomena. Of particular interest would be the anomalous behavior of the NMR parameters of trimethylamine–borane and –haloborane adducts.

Acknowledgment. The authors wish to thank the National Research Council of Canada for financial support.

Registry No. $Me_3N{\cdot}BF_3$, 420-20-2; $Me_3N{\cdot}BF_2Cl$, 25889-87-6; $Me_3N{\cdot}BF_2Br$, 25889-93-4; $Me_3N{\cdot}BF_2I$, 25889-95-6; $Me_3N{\cdot}BFCl_2$, 25889-88-7; $Me_3N{\cdot}BFClBr$, 39708-26-4; $Me_3N{\cdot}BFClI$, 39708-27-5; $Me_3N{\cdot}BFBr_2$, 25889-94-5; $Me_3N{\cdot}BFBrI$, 39708-28-6; $Me_3N{\cdot}BCl_3$, 1516-55-8; $Me_3N{\cdot}BFI_2$, 25889-96-7; $Me_3N{\cdot}BCl_2Br$, 25889-90-1; $Me_3N{\cdot}BCl_2I$, 25889-97-8; $Me_3N{\cdot}BClBr_2$, 25889-91-2; $Me_3N{\cdot}BClBrI$, 39708-29-7; $Me_3N{\cdot}BBr_3$, 1516-54-7; $Me_3N{\cdot}BClI_2$, 25889-98-9; $Me_3N{\cdot}BBr_2I$, 39708-24-2; $Me_3N{\cdot}BBrI_2$, 39708-25-3; $Me_3N{\cdot}BI_3$, 5041-59-8; ^{13}C, 14762-74-4; ^{11}B, 14798-13-1.

References and Notes

(1) A. F. Fratiello, G. A. Vidulich, and R. E. Schuster, *J. Inorg. Nucl. Chem.*, **36**, 93 (1974).
(2) R. A. Geanangel, *Inorg. Chem.*, **14**, 696 (1975).
(3) J. M. Miller and M. Onyszchuk, *Can. J. Chem.*, **42**, 1518 (1964); **44**, 899 (1966).
(4) B. Benton-Jones, M. E. A. Davidson, J. S. Hartman, J. J. Klassen, and J. M. Miller, *J. Chem. Soc., Dalton Trans.*, 2603 (1972).
(5) J. S. Hartman and J. M. Miller, *Inorg. Nucl. Chem. Lett.*, **5**, 831 (1969).
(6) J. S. Hartman and J. M. Miller, *Inorg. Chem.*, **13**, 1467 (1974).
(7) B. W. Benton and J. M. Miller, *Can. J. Chem.*, **52**, 2866 (1974).
(8) H. Binder and E. Fluck, *Z. Anorg. Allg. Chem.*, **381**, 116 (1971).
(9) J. M. Miller, unpublished observations.
(10) P. J. Clippard and R. C. Taylor, *Inorg. Chem.*, **8**, 2802 (1969).
(11) G. R. Eaton and W. N. Lipscomb, "NMR Studies of Boron Hydrides and Related Compounds", W. A. Benjamin, New York, N.Y., 1969.
(12) T. Vladimiroff and E. R. Malinowski, *J. Chem. Phys.*, **46**, 1830 (1967).
(13) J. S. Hartman and G. J. Schrobilgen, *Inorg. Chem.*, **11**, 940 (1972).
(14) B. F. Spielvogel and J. M. Purser, *J. Am. Chem. Soc.*, **93**, 4418 (1971).
(15) E. R. Malinowski, *J. Am. Chem. Soc.*, **91**, 4701 (1969).
(16) E. R. Malinowski and T. Vladimirov, *J. Am. Chem. Soc.*, **86**, 3575 (1969).
(17) T. Vladimiroff and E. R. Malinowski, *J. Chem. Phys.*, **42**, 444 (1965).
(18) R. G. Kidd and H. G. Spinney, *J. Am. Chem. Soc.*, **45**, 88 (1973); *Inorg. Chem.*, **12**, 1967 (1973).

Contribution from the Department of Chemistry, Vanderbilt University, Nashville, Tennessee 37235

Use of Pseudopotential Theory to Study Molecular Structure. II. A NOCOR (Neglect of Core Orbitals) Calculation of the P_4 and P_2 Molecules and Their Interconversion

ROMAN OSMAN, PATRICK COFFEY, and JOHN R. VAN WAZER*

Received July 14, 1975 AIC50493A

The new (NOCOR) valence-only ab initio LCAO–MO–CSF method, in which the effect of the core electrons is represented by a local model potential and a nonlocal pseudopotential, has been applied to the P_2 and P_4 molecules and is found to give results for a minimum-Slater representation (in which only s and p atomic functions are employed) that are comparable to those from full-core calculations. Optimization of the molecular geometry for this representation also leads to good results. Upon adding d functions, it is found that the electronic hybridization of each phosphorus atom in the P_4 molecule goes from $s^{1.90}p^{3.10}$ to $s^{1.77}p^{3.08}d^{0.15}$, resulting in considerable polarization of the valence electronic distribution with the total electronic charge shifting away from the atoms into the center of the P_4 tetrahedron and also into the P–P axial regions. The enthalpy and an activation energy have been calculated for a symmetry-allowed dissociation of P_4 into $2P_2$, a process which was followed in detail with bond distance optimization.

Introduction

There are still many problems, covering the full range from preparative through theoretical chemistry, concerned with the variety and structures of the allotropic forms[1] of phosphorus. For example, the role of d atomic orbitals in the electronic structure of the P_4 tetrahedral molecule has been a central issue discussed in two recent papers[2-4] describing ab initio SCF computations on this molecule. However the size of the basis set required for inclusion of d character was sufficiently large so as to be precluded from actual calculation in both papers. Our recently developed[5-7] NOCOR procedure for carrying out ab initio SCF computations for only the valence orbitals offers a way of readily incorporating[5] d character into the LCAO description of the P_4 molecule and such work is reported herein.

Although there is a near-Hartree–Fock computation[8] available for the P_2 molecule, the relationship between the electronic structures of the P_2 and P_4 molecules has not been investigated previously. Therefore we have recalculated the P_2 molecule in a valence-only minimum-Slater basis set and have mathematically simulated the process of pulling apart a P_4 molecule into two P_2 molecules in a symmetry-allowed fashion.

Calculational Details

The previously described[5-7] procedure was employed for carrying out LCAO–MO–SCF computations on the valence orbitals of the molecules under study, using an adaptation of the Phillips–Kleinman pseudopotential to replace orthogonality constraints along with an exponential screening function to replace the core–valence Coulombic and exchange interactions. An atom-optimized[9] minimum-Slater basis set in which each orbital was described by three Gaussian functions,[10] i.e., STO-3G, was employed; and, for introducing d character, a sixfold single-Gaussian set of d functions was used with an exponent chosen as previously described.[11] A Slater function expressed in terms of six Gaussian functions was used to delineate each atom symmetry type in the core; but, of course, these core functions are not part of the basis set since they serve only to define the pseudopotential.

Results and Discussion

NOCOR vs. Full SCF. Since the NOCOR method is still quite new, we believe it is desirable to compare the results obtained with it to those from regular full-SCF calculations, particularly when about the same basis set was employed. In Table I a series of properties is reported for the P_2 molecule using the NOCOR method, a reasonably comparable minimum-Slater calculation,[12,13] and a near-Hartree–Fock computation.[8] A similar comparison for the P_4 molecule of the NOCOR results with minimum-Slater findings[2] and the results from a rather large Gaussian calculation[4] (equivalent to a single-ζ description for the core and a double-ζ description for the valence shell) are reported in Table II. In both tables,

Table I. Intercomparison of Results for the P_2 Molecule

Property	NOCOR[a] with d	Min Slater with d[b]	Exten Slater with d and f[c]	Exptl
P–P distance, Å	1.924		1.851	1.894[d]
Spectroscopic data				
ω, cm^{-1}	858.1		919.7	780.4[e]
$\omega\chi$	3.23		3.88	2.804
B_e	0.294		0.318	0.3033
α_e, cm^{-1}	0.00086		0.00102	0.00142
Orbital energies, eV				
$4\sigma_g$	−22.43	−23.86	−24.79	
$4\sigma_u$	−15.22	−15.68	−16.38	
$5\sigma_g$	−10.11	−11.55	−11.13	
$2\pi_u$	−8.96	−10.67	−10.26	

[a] This study; NOCOR minimum STO-3G augmented with a single set of Gaussian d orbitals; atom-optimized s and p exponents. [b] See ref 12 and 13; minimum STO augmented with a single set of Slater d orbitals; Slater-rule s and p exponents. [c] See ref 8; extended STO using d and f functions; atom-optimized s and p exponents. [d] See ref 14. [e] See ref 15.

Table II. Intercomparison of Results for the P_4 Molecule

Property	NOCOR with d[a]	NOCOR without d[b]	Min Slater without d[c]	Gaussian without d[d]	Exptl
P–P distance, Å		2.381	2.360		2.210[e]
$\omega(A_1$ str), cm^{-1}		597			619 ± 5[f]
$k(A_1$ str), mdyn/Å		2.44			2.19 ± 0.02
$\Delta H_0^\circ(P_4 \rightarrow 2P_2)$, kcal/mol		25	45		54.05,[g] 53.71[h]
Orbital energies, eV					
$4a_1$	−26.11	−25.98	−30.30	−31.50	
$5t_2$	−17.94	−18.57	−19.95	−21.00	
$5a_1$	−11.42	−10.78	−11.64	−12.45	−11.85[i]
$6t_2$	−9.82	−9.77	−10.39	−11.15	−10.47
2e	−9.06	−9.02	−9.71	−10.46	−9.72

[a] This study; NOCOR minimum STO-3G augmented with a single set of Gaussian d orbitals; atom-optimized s and p exponents. [b] This study; NOCOR minimum STO-3G, with atom-optimized s and p exponents. [c] See ref 2; minimum STO-3G, with atom-optimized s and p exponents. [d] See ref 4; contracted (sp) GTO's equivalent to a single-ζ description for the core and a double-ζ description for the valence shell, with atom optimization of the exponents and contraction coefficients. [e] See ref 14. [f] See ref 16. [g] See ref 17. [h] See ref 15. [i] See ref 4.

experimental values[14-17] are also presented when available. It can be seen from both Tables I and II that the NOCOR method gives respectable results for optimization of bond distances and spectroscopic data. The orbital energies are also quite good, being consistently somewhat higher than the full-core results. As might be expected, a generally better fit is found between the NOCOR calculation, which corresponds to a minimum-Slater representation (with or without added d character), and a full-core minimum-Slater calculation, as compared to the NOCOR vs. an extended-base calculation.

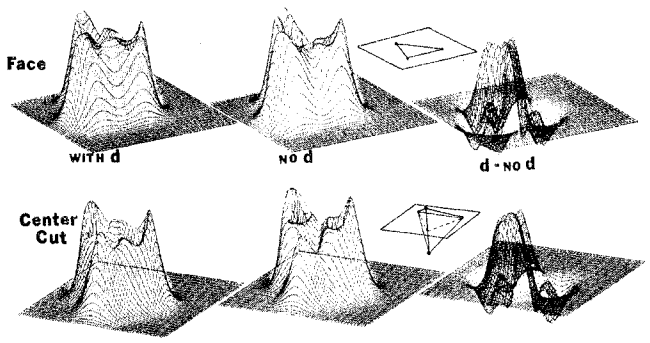

Figure 1. Cross-sectional electron density plots in which the total electron density is plotted perpendicular to the chosen plane, which passes through a face of the P_4 molecule for the top row and through an edge (to the rear) and the center of the molecule for the bottom row. The left-hand plots depict the NOCOR results with d functions added, and the center plots shows the same calculation without d character. The right-hand plots present the difference (d − no-d), at a fivefold magnification of the electron scale in a transparent representation.

Electronic Structure of the P_4 Molecule. Highly symmetrical molecules such as tetraphosphorus are particularly interesting in that they may be viewed differently from various vantage points. For example, the upper left-hand electron density diagram of Figure 1 corresponds to the total electron density of the P_4 molecule as depicted for a cut through one of its faces, each of which contain three phosphorus atoms. On the other hand, the lower left-hand diagram of Figure 1 shows (in the same mathematical representation) a cut through the middle of the P_4 tetrahedron passing through a pair of neighboring phosphorus atoms and bisecting the line connecting the remaining two phosphorus atoms. A similar change of orientation may be carried out with a Mulliken population analysis, thereby shifting electronic charge from one category to another while the total charge for any atomic contribution remains constant. In Table III, a population analysis is reported for a P_4 phosphorus atom with respect to one of its P–P bond axes, to which the σ and the π notations are referred. In Table IV, the population analysis is carried out with respect to a C_3 axis passing through the selected phosphorus atom and the center of the tetrahedron. Note in both cases that the gross population of the spherically symmetrical s_σ atomic orbitals of the phosphorus atom in question is necessarily the same for a particular orbital described in a given basis set, whereas the proportioning of the p electrons

Table III. Mulliken Population Analysis of the P_4 Molecule with Respect to a P–P Bond Axis[a]

Mol orbital	Gross population of a P atom						P–P overlap population		
	s_σ	p_σ	p_π[b]	d_σ	d_π[b]	d_δ[b]	σ_{total}	π_{total}[b]	δ[b]
$4a_1$	0.415	0.051	0.026	0.003	0	0.006	0.164	0.003	0.000
	(0.393)	(0.071)	(0.036)				(0.170)	(0.003)	
$5t_2$[c]	1.143	0.058	0.249	0.020	0.0025	0.005	0.088	0.034	0
	(1.224)	(0.037)	(0.239)				(−0.019)	(0.012)	
$5a_1$	0.085	0.264	0.132	0.007	0	0.013	−0.010	0.040	0.002
	(0.107)	(0.262)	(0.131)				(−0.018)	(0.030)	
$6t_2$[c]	0.127	0.552	0.786	0.017	0.019	−0.001	0.134	−0.025	−0.000
	(0.174)	(0.556)	(0.771)				(0.111)	(−0.037)	
2e[d]	0	0.160	0.800	0.013	0.020	0.007	0.127	−0.035	0.001
	(0)	(0.167)	(0.833)				(0.109)	(−0.046)	

[a] The σ, π, and δ notations refer to the P–P internuclear axis involving the atom(s) for which electronic population data are presented. The values in parentheses refer to the calculation without d orbitals. [b] This includes both of the set of π (or δ) functions. [c] The contributions from each of the triply degenerate orbitals are summed. [d] The contributions from the doubly degenerate orbitals are summed.

Table IV. Mulliken Population Analysis of the P_4 Molecule with Respect to a "Center-Bond" Axis[a]

Mol orbital	Gross population of a P Atom						P-P overlap population[b]		
	s_σ	p_σ	p_π[c]	d_σ	d_π[c]	d_δ[c]	σ_{total}	π_{total}[c]	δ[c]
$4a_1$	0.415	0.076	0	0.009	0	0	0.167	0	0
	(0.393)	(0.107)	0				(0.173)	(0)	
$5t_2$[d]	1.143	0.014	0.294	−0.001	0.047	0.003	0.103	0.019	−0.000
	(1.227)	(−0.017)	(0.293)				(−0.018)	(0.011)	
$5a_1$	0.085	0.395	0	0.020	0	0	0.031	0	0
	(0.107)	(0.393)	0				(0.012)	(0)	
$6t_2$[d]	0.127	0.658	0.680	−0.003	0.036	0.002	0.055	0.054	0.000
	(0.174)	(0.669)	(0.657)				(0.035)	(0.039)	
2e[e]	0	0	0.960	0	0.012	0.027	0.175	−0.083	0.000
	(0)	(0)	(1.000)				(0.154)	(−0.091)	

[a] The σ, π, and δ notations refer to the axis passing through the chosen phosphorus atom and the center of the P_4 molecule. The values in parentheses refer to the calculation of P_4 without d orbitals. [b] These values correspond to one-third of the overlap of the chosen phosphorus atom with the three other phosphorus atoms. [c] This includes both of the set of π (or δ) functions. [d] The contributions from each of the triply degenerate orbitals are summed. [e] The contributions from the doubly degenerate orbitals are summed.

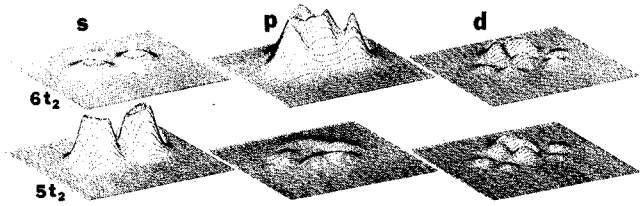

Figure 2. Cross-sectional electron density plots showing (left to right) the separated s, p, and d contributions to the degenerate set of $5t_2$ (lower row) and $6t_2$ (upper) molecular orbitals of the P_4 tetrahedron. The basal plane of these plots passes through an edge (to the front) and the center of the molecule, and the electron density scale for the d plots is magnified 5 times over that for the plots of the s and p contributions.

between the σ and π categories is necessarily different, as is also the situation with respect to the distribution of the d atomic orbitals among the σ, π, and δ categories. Similarly the P–P overlap population must be distributed differently among the σ, π, and δ symmetries when these terms have different reference axes, as is the case for Table III vs. Table IV.

Like Galileo with the solar system, we believe that it is meaningful to consider which choice of coordinates leads to the simplest description. From inspection of Tables III and IV, it is apparent that the concept of four-center bonding as holding the P_4 tetrahedron together represents a mathematically simpler picture of the molecule with respect to molecular orbitals $4a_1$ and $5a_1$ and the 2e set than does the representation of this molecule in terms of a network of P–P bonds ("bent" or "unbent") running along the six edges of the tetrahedron. However, the two sets of t_2 orbitals ($5t_2$ and $6t_2$) exhibit both p_σ and p_π character in both the P–P and four-center bond representations.

In order to understand better the nature of the degenerate orbitals $5t_2$ and $6t_2$, their atomic s, p, and d contributions have each been separately plotted in Figure 2 for the calculation involving the d functions. Although the $(s_\sigma - s_\sigma)$ overlap is antibonding (−0.447 for the $5t_2$ set and −0.074 for the $6t_2$ set), the left-hand plot of Figure 2 shows bonding along the P–P axis which must be overweighed by antibonding elsewhere (predominantly in the center of the tetrahedron). According to Table IV the "center-bond" p_σ contribution to the population of the $6t_2$ set is about twice that of each p_π orbital, and this shows up in the $6t_2$ middle plot of Figure 2 in the fact that the height representing the p electron density along the center-bond axis is about twice that of the ridges forming valleys on either side of the phosphorus nucleus. Furthermore, the middle plot in this figure for the $5t_2$ set shows that the "center-bond" p_π far outweighs the p_σ contribution and that both are small, as also can be observed in Table IV. Thus, we see that, although complicated, the orbitals of t_2 symmetry

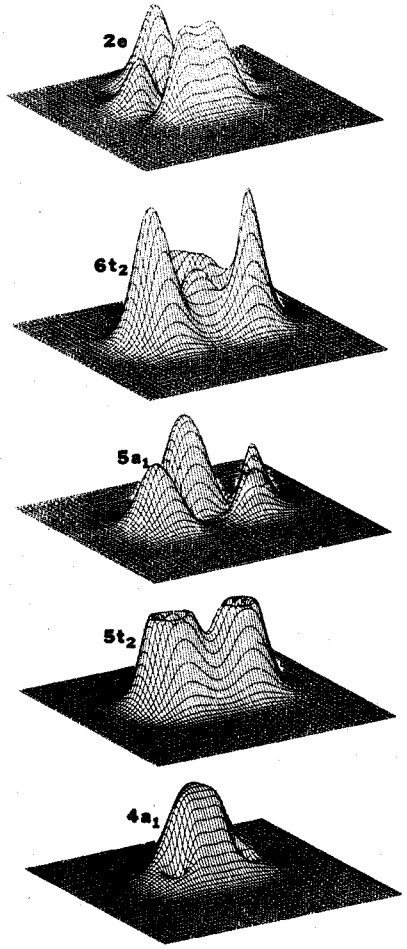

Figure 3. Cross-sectional electron density plots of each of the filled valence-shell molecular orbitals or complete sets of degenerate orbitals of the P_4 molecule, with the basal plane of the plots passing through an edge (to the front) and the center of the tetrahedral molecule.

can also be treated comfortably from the "center-bond" point of view.

Electron density plots of the five filled symmetry orbital sets making up the valence shell of the P_4 molecule are shown in Figure 3, which represents a cut through a pair of phosphorus atoms, with the plane of the cut also bisecting the P–P axis of the remaining two phosphorus atoms in the molecule.[12] Therefore, these electron density diagrams include two of the four "center-bond" axes as well as one of the six P–P bond axes. Note that the basal planes of the plots shown in Figure 3 are rotated 120° (in the plane) from the plots presenting the same cut that are depicted in the bottom row of Figure

1. From Figure 3, it is clear that orbital $4a_1$ does indeed represent overlap in the central portion of the tetrahedral molecule of the s valence orbitals of all four phosphorus atoms, whereas, orbital $5a_1$ corresponds to similar p_σ four-center bonding (with some s and d character) representing mainly a nonbonding arrangement with pronounced lone-pair character. The pair of 2e orbitals is clearly seen in Figure 3 to be p_π populated with respect to a "center-bond" axis. However, since the C_3 axes meet at an angle in the center of the tetrahedron, there cannot be π bonding so that the overlap of these p_π orbitals must correspond to σ bent bonds, as indicated in Table IV.

As shown in Figure 2, the $5t_2$ and $6t_2$ sets are similar in makeup, with s antibonding predominating in $5t_2$ and p bonding in $6t_2$. Since the p and d contributions to the $5t_2$ set are small (Figure 2), this set is only slightly bonding and primarily exhibits s-type lone-pair character. The $6t_2$ set, having a large p bonding contribution, forms what might be called an "inwardly bent bond" which involves all three p-type atomic orbitals of each phosphorus atom so that the charge density of each atom may be likened to a hollow prolate ellipsoid with dense ends, having as its principal axis a C_3 axis of the molecule.

Effect of d Character on the P_4 Molecule. Generally the addition of d functions to an sp basis set changes the electron density distribution so slightly as to be practically imperceptible when plots representing the total electron density before and after addition of d character are directly intercompared. However, this is not the case for the P_4 molecule in which the effect on the total electron-density distribution upon adding d character is pronounced, as can be seen in Figure 1. Reading from left to right, the plots in this figure correspond to the calculation with d orbitals, without d orbitals, and a difference plot (d − no-d) in which the effect of adding d character is shown on an electron density scale which is magnified 5 times as compared to those of the other plots. In the top row of plots presented in Figure 1 which depicts a P_3 plane making up one of the four faces of the P_4 tetrahedron, there is a pronounced hill between each of the pairs of phosphorus atoms when d character is allowed as compared to a valley for the calculation without d orbitals.

In the plots of the second row of Figure 1, corresponding to a cut passing through a P_2 edge of the tetrahedron and bisecting the P–P axis of the other P_2, inclusion of d character leads to an increased electron density along the P–P bond axis as indicated by the increased height of the front peak and the shoulder between the phosphorus atoms in the left-hand plot in comparison to the middle diagram. The difference plots show this effect and also emphasize the fact that addition of d orbitals leads to a transfer of charge from the phosphorus lone-pair regions to the center (as well as to the edges) of the P_4 tetrahedron.

The effect of adding d character on shifting the electron density shows up in all of the filled valence-shell molecular orbitals, being least pronounced in the most stable of these. Electron density plots show that for the pair of 2e orbitals, addition of a d manifold to the basis set results in transfer of charge from the ends toward the center of what is clearly a P–P σ bond, whereas, for the $6t_2$ orbital triplet as well as for orbital $5a_1$, the concomitant electron shift is from the lone-pair region toward the center of the tetrahedron. On the other hand, for the triply degenerate $5t_2$ set of orbitals and the $4a_1$ orbital, the shift of electronic charge upon allowing d character is essentially the reverse of this, being from the center region to the regions outside of the tetrahedron along each of the four C_3 axes. As exemplified by the plots of the d-function contributions to molecular orbital sets $5t_2$ and $6t_2$ in Figure 2, the d orbitals themselves are so disposed that they can be readily analyzed in terms of center bonding, as is the case for the whole molecular orbital set.

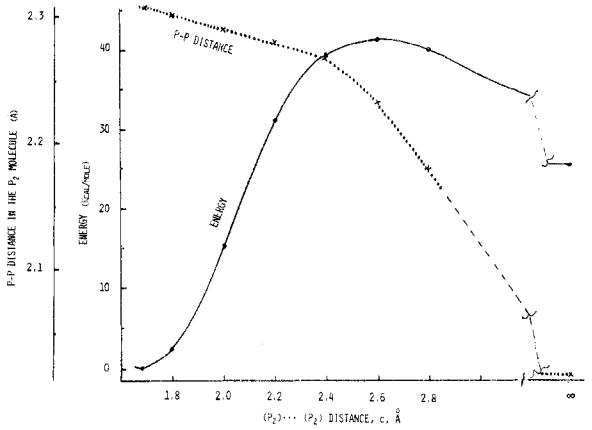

Figure 4. Variation of total energy and optimized closest P–P distances upon pulling a P_4 molecule apart along a C_2 axis. The distance, c, on that axis between the resulting P_2 pairs is presented as the horizontal coordinate.

The population analyses in Tables III and IV show that the d contributions to the gross population of any of the phosphorus atoms with respect to each of the molecular orbitals is quite small, although the incorporation of d character had a quite large effect on the distribution of the s and p character between the various molecular orbitals. It also greatly affects the overlap population, particularly in the triply degenerate set of $5t_2$ orbitals which was converted from a set exhibiting a small amount of antibonding to one of the stronger bonding orbital sets by the incorporation of d character.

$P_4 \rightarrow 2P_2$. The dissociation of P_4 into $2P_2$ was studied by pulling the two constituent P_2 groups apart along an axis that passes through the centers of opposite P–P bonds in the P_4 molecule. For each distance c between the two P–P bonds,

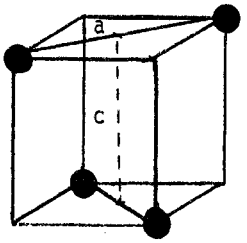

the P–P distance, a, was varied so as to obtain the minimum energy. The energy of the system during the dissociation is shown in Figure 4 along with the optimized P–P distance.

The transition state for the dissociation occurs at c = 2.6 Å, with a = 2.23 Å. The enthalpy of activation at 0 K (ΔH_0^*) for the process $P_4 \rightarrow 2P_2$ as calculated from the difference between the energies of the transition state and the ground state (P_4) is 41.1 kcal/mol. The calculated enthalpy of activation for the reverse process ($2P_2 \rightarrow P_4$) is 15.9 kcal/mol.

Figure 5 is the correlation diagram of the process. It clearly shows that the process is symmetry allowed, as none of the molecular orbitals of the same symmetry exhibit crossing. Upon dissociation, the T_d symmetry of the P_4 molecule changes into D_{2d} symmetry, thus causing splitting of the doubly (e) and triply (t) degenerate representations. The e representation splits into a_1 and b_1 representations; t_2, into b_2 and doubly degenerate e; and t_1, into a_2 and doubly degenerate e.

Upon total dissociation, molecular orbital $4a_1$ and one component of $5t_2$ ($5b_2$ in D_{2d}) of the P_4 molecule become the two $4\sigma_g$ of the pair of P_2 molecules. The second part of $5t_2$ (6e in D_{2d}) becomes the two $4\sigma_u$ orbitals of the pair of P_2 molecules. The same phenomenon takes place with $5a_1$ and

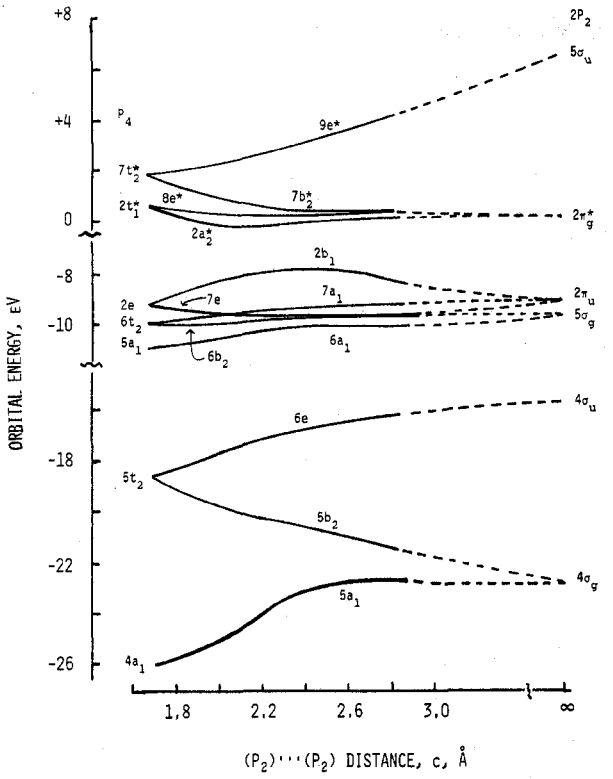

Figure 5. Molecular orbital correlation chart relating the orbitals of the P_4 molecule (left-hand side) to those of the pair of P_2 molecules (right-hand side) upon pulling a P_4 molecule apart along a C_2 axis. The distance, c, on that axis between the resulting P_2 pairs is presented as the horizontal coordinate.

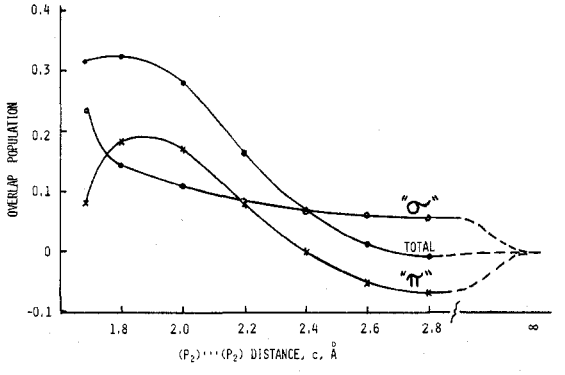

Figure 6. The overlap population between two phosphorus atoms which end up in different P_2 molecules when the P_4 molecule is pulled apart along a C_2 axis. The distance, c, on that axis between the resulting P_2 pair is presented as the horizontal coordinate. The terms "σ" and "π" refer to the sum of the overlap values for the molecular orbitals that transform (see Figure 5) into orbitals of that symmetry in the resulting P_2 molecules.

one component of $6t_2$ ($6b_2$ in D_{2d}) giving $5\sigma_g$, and the 9e* (in D_{2d}) of $7t_2$* giving $5\sigma_u$*. The 7e (in D_{2d}) component of $6t_2$ and the 2e which is split into $7a_1$ and $2b_1$ (in D_{2d}) become the two sets of doubly degenerate $2\pi_u$. The $2t_1$* and the $7b_2$* (in D_{2d}) component of $7t_2$* become $2\pi_g$*.

Figures 6 and 7, respectively, describe, as a function of the distance c, the overlap between a pair of phosphorus atoms which separate into the two different P_2 molecules and the overlap between a pair which stays together to form a P_2 molecule.

As may be seen from Figure 6, the total P–P overlap between a separating pair of phosphorus atoms increases by a slight amount upon small distortion of the tetrahedron; then it decreases monotonically to zero for larger c values. The total overlap may be divided into "σ" and "π" overlap contributions.

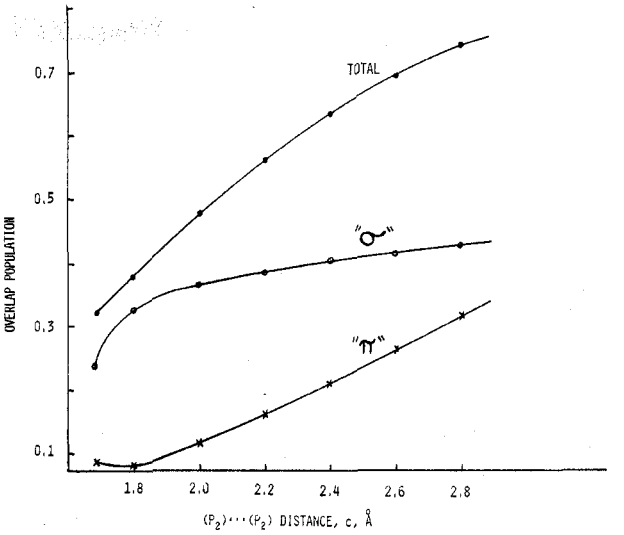

Figure 7. The overlap population between two phosphorus atoms which remain together to form a P_2 molecule upon pulling a P_4 molecule apart along a C_2 axis. The distance, c, on that axis between the resulting P_2 pair is presented as the horizontal coordinate. The terms "σ" and "π" refer to the sum of the overlap values for the molecular orbitals that transform (see Figure 5) into orbitals of that symmetry in the resulting P_2 molecules.

(By the "σ" and "π" notation we mean in this case the overlap in the molecular orbitals which become σ and π, respectively, in the P_2 molecules.) The "σ" overlap is seen in Figure 6 to decrease smoothly to zero; whereas the "π" overlap shows an increase for small distortions followed by a sharp decrease for larger c values to a negative overlap, which must go to zero for infinite separation of the two P_2 molecules. This suggests that the "σ" structure is broken uniformly. However, the "π" structure strengthens at small distortions and then dominates the repulsive interaction between the two P_2 molecules when separated by the van der Waals distance. The maximum in the total overlap which appears for a slightly distorted P_4 molecule may be attributable to strain relief and is an example of the fact that maximum stability does not necessarily occur at maximum overlap.

The P–P overlap shown in Figure 7 reveals a uniform increase in the total overlap during the dissociation process due to the formation of the triple bond in diphosphorus. The "σ" overlap increases sharply at the beginning and then rises slowly as c is increased. The "π" overlap decreases slightly at the beginning and then increases constantly as the two P_2 molecules are drawn apart.

Viewing the data of Figure 6 with respect to association of a pair of diphosphorus molecules, we see that, when the two P_2 molecules come together along the chosen path, the initial repulsion is due to the interaction of the π orbitals of each diatomic molecule——with the concomitant interaction between the σ orbitals being attractive. As the pair of P_2 molecules move together even closer, the repulsion between their π orbitals turns into attraction. And, finally, as the pair of P_2 molecules fuse together to form the P_4 tetrahedron, the orbitals which exhibited π character in the separated diatomic molecules now contribute less to the overlap than the orbitals which were originally σ, with the latter rapidly dominating the bonding in the final stage of the association process.

Discussion

The ease with which the electronic structure of the P_4 molecule may be interpreted in terms of center bonding indicates that this structure is dominated by the cyclical cage arrangement of the four phosphorus nuclei. Inspection of electron density plots[18] of cyclopropane shows a similarity between the valence molecular orbitals of this molecule and

of the P_4 molecule. Thus, orbitals $2a_1'$ and $3a_1'$ of C_3H_6 strikingly resemble orbitals $4a_1$ and $5a_1$ of P_4, and there is also a relationship between the 2e' set of C_3H_6 and the $5t_2$ set of P_4 and between the 3e' set of C_3H_6 and the $6t_2$ set of P_4. These similarities are attributable to the three-atom ring structures of both molecules.

The valence electronic structure of highly symmetrical molecules exhibiting an essentially spherical shape will have the same nodal surfaces in the valence region as are to be found for an isoelectronic atom. For example, the $2a_1$ and the triply degenerate set of $1t_2$ molecular orbitals making up the filled valence shell of the methane molecule[18] exhibit the nodal structures of a 2s and a triply degenerate 2p set of atomic orbitals of neon. The tetrahedral structure of the P_4 molecule, being spherelike, should in like manner also cause the valence molecular orbitals of this molecule to exhibit pseudoatomic character. We find that orbital $4a_1$ of P_4 exhibits no nodal planes and a central concentration of charge so that it is the lowest valence s orbital of the pseudoatom. Likewise each molecular orbital of the triply degenerate $5t_2$ set has a molecular nodal plane and these three nodal planes are mutually perpendicular, so that the $5t_2$ orbitals of P_4 are pseudoatomic p orbitals. Molecular orbital $5a_1$ has a single spherical nodal surface which passes through all four phosphorus atoms. Thus from the pseudoatomic viewpoint, this is the next higher s-type pseudoatomic orbital beyond molecular orbital $4a_1$.

Orbitals $6t_2$ and 2e correspond to a fivefold set of pseudoatomic d orbitals, with each orbital of this set exhibiting the proper pair of nodal surfaces. In accord with ligand-field theory, the tetrahedral geometry of the P_4 molecule causes this fivefold set to split into a triply degenerate set of T_2 symmetry and a doubly degenerate set of E symmetry as observed. The repulsive effect of the filled-valence-shell ligands on a centrally located transition metal atom in a complex causes its t_2 set of d orbitals to exhibit a higher energy than the e set. However, for the P_4 molecule where the "ligand" positions contribute all of the electronic charge with none coming from a central atom, the situation must be reversed, with the e orbitals lying above the t_2 orbitals as observed. The calculated splitting between the t_2 and e sets, Δ_t, of 6730 cm^{-1} for the pseudoatom character of the P_4 molecule has, of course, no spectrographic significance because both the $6t_2$ and 2e levels are completely filled.

Acknowledgment. We wish to thank the Air Force Office of Scientific Research for partial support of this work under Grant AFOSR 72-2265.

Registry No. P_2, 12185-09-0; P_4, 12185-10-3.

References and Notes

(1) J. R. Van Wazer, "Phosphorus and Its Compounds", Vol. I, Interscience, New York, N.Y., 1958.
(2) M. F. Guest, I. H. Hillier, and V. R. Saunders, *J. Chem. Soc., Faraday Trans. 2*, **68**, 2070 (1972).
(3) I. H. Hillier and V. R. Saunders, *Chem. Commun.*, 1233 (1970).
(4) C. R. Brundle, N. A. Kuebler, M. B. Robin, and H. Basch, *Inorg. Chem.*, **11**, 20 (1972); also see R. R. Hart, M. B. Robin, and N. A. Kuebler, *J. Chem. Phys.*, **42**, 3631 (1965).
(5) P. Coffey, C. S. Ewig, and J. R. Van Wazer, *J. Am. Chem. Soc.*, **97**, 1656 (1975).
(6) C. S. Ewig, P. Coffey, and J. R. Van Wazer, *Inorg. Chem.*, **14**, 1848 (1975).
(7) C. S. Ewig and J. R. Van Wazer, *J. Chem. Phys.*, **63**, 4035 (1975).
(8) R. S. Mulliken and B. Liu, *J. Am. Chem. Soc.*, **93**, 6738 (1971).
(9) E. Clementi and D. L. Raimondi, *J. Chem. Phys.*, **38**, 2686 (1963).
(10) R. F. Stewart, *J. Chem. Phys.*, **52**, 431 (1970).
(11) I. Absar and J. R. Van Wazer, *Chem. Phys. Lett.*, **11**, 310 (1971).
(12) D. B. Boyd and W. N. Lipscomb, *J. Chem. Phys.*, **46**, 910 (1967).
(13) D. B. Boyd, *J. Chem. Phys.*, **52**, 4846 (1970).
(14) L. E. Sutton, Ed., *Chem. Soc., Spec. Publ.*, **No. 11** (1958).
(15) *Natl. Stand. Ref. Data Ser., Natl. Bur. Stand.*, **No. 37** (1971).
(16) R. S. McDowell, *Spectrochim. Acta, Part A*, **27**, 773 (1971).
(17) D. D. Wagman et al., *Natl. Bur. Stand. (U.S.), Tech. Note*, **No. 270-3** (1968).
(18) J. R. Van Wazer and I. Absar, "Electron Densities in Molecules and Molecular Orbitals", Academic Press, New York, N.Y., 1975.

Contribution from the Lash Miller Chemistry Laboratories and Erindale College, University of Toronto, Toronto, Ontario, Canada

A Reinvestigation of the Optical Spectra of Nickel, Palladium, and Platinum Atoms in Noble Gas Matrices

W. KLOTZBÜCHER and G. A. OZIN*

Received May 13, 1975 AIC504739

Optical spectra from 200 to 700 nm have been obtained for Ni, Pd, and Pt atoms in Ar, Kr, and Xe matrices at 6–8 K. The spectra for Ni and Pt atoms in Ar agree quite well with the earlier data in Ar matrices for the strongest lines. The corresponding data obtained in Kr and Xe matrices supplement the Ar data and correlate reasonably well with the reported gas-phase atomic transitions although the matrix shifts for Pt in Xe seem anomalously large. On the other hand, the previously reported optical spectrum of Pd atoms in Ar matrices, which displayed absorptions above 290 nm, is proven to have originated not from isolated Pd atoms but rather from the products of the reaction of Pd atoms with air impurities, the most intense absorptions of which are shown to be associated with $Pd(N_2)$ and $Pd(N_2)_2$ complexes. The genuine spectrum of atomic Pd in Ar, Kr, and Xe matrices is established as an extremely intense group of lines below 250 nm. The atomic transitions of Pd exhibit blue matrix shifts, in agreement with the predictions of AMCOR. An amonotonic trend is noted for the matrix-induced frequency shifts of Pd and Pt atoms in noble gas matrices ($\Delta\nu_{Xe} > \Delta\nu_{Ar} > \Delta\nu_{Kr}$) whereas a monotonic trend is seen for Ni atoms ($\Delta\nu_{Ar} > \Delta\nu_{Kr} > \Delta\nu_{Xe}$). This is taken to indicate a substantial metal–matrix interaction between the most polarizable (class B) metals and Xe, suggestive of weak "complex" formation.

Introduction

One of the simplest ways of determining the fate of a metal atom when cocondensed with an inert gas or a reactive species diluted in an inert gas is to investigate its optical spectrum. Although experimentally straightforward, the spectra can be complicated through metal atom–matrix interactions which include the shifting and broadening of spectral lines, and crystal field, spin–orbit, and multiple trapping site splitting effects. The work of Mann and Broida,[1] Brewer,[2] and Gruen[3] recently demonstrated that the observation of matrix shifts for the transitions of metal atoms isolated in noble gas matrices relative to those of the gaseous metal atom was a general phenomenon and that these shifts could be as large as several thousand wavenumbers. However, reasonable correlations between the strongest atomic transitions can be made by appropriately shifting the entire matrix spectrum from the respective gas-phase values.

Although no universal theory has been proposed to explain